ISSN 0036-0244, Russian Journal of Physical Chemistry A, 2022, Vol. 96, No. 13, pp. 86–91. © Pleiades Publishing, Ltd., 2022.

PHYSICAL CHEMISTRY OF SOLUTIONS

Tribocorrosion Behaviors of NiTi/$AlNi_2Ti$ Intermetallic Alloy in NaCl Solution

J. X. Zhang[a], B. N. Liang[a],*, and X. R. Guo[a]

[a] *School of Material Engineering, Lanzhou Institute of Technology, Lanzhou, 730050 China*

* *e-mail: liangbn168134@163.com*

Received December 21, 2021; revised December 21, 2021; accepted February 20, 2022

Abstract—A novel NiTi/$AlNi_2Ti$ ternary intermetallic alloy were prepared by arc melting. Tribocorrosion behaviors of the NiTi/$AlNi_2Ti$ alloy were investigated by tribocorrosion tests. The results showed that NiTi/$AlNi_2Ti$ alloy had an excellent tribocorrosion resistance in NaCl solution and is more suitable as a tribocorrosion resistant material than 1Cr18Ni9Ti stainless steel. With the onset of sliding, the OCP of NiTi/$AlNi_2Ti$ alloy decreases and the corrosion current density increases during tribocorrosion test, and the decrease of the OCP is proportional to the increase of the frictional force, showing a strong corrosion-wear synergy effect. The corrosion current density and wear loss volume of the NiTi/$AlNi_2Ti$ alloy increase with the increase of applied potentials.

Keywords: intermetallics, NiTi/$AlNi_2Ti$ alloy, corrosion, ribocorrosion behaviors

DOI: 10.1134/S0036024422130271

INTRODUCTION

Corrosion and wear are the two most frequently encountered failure modes of mechanical components working under extreme conditions [1]. Moreover, corrosion and wear two failure modes coexist in many engineering fields, and their interaction usually leads to accelerated failure of materials [2, 3]. Commonly used corrosion resistant materials such as stainless steel and conventional wear resistant materials such as cast iron and high carbon steel are not always able to meet the requirements of corrosion and wear resistance simultaneously [4]. Therefore, it is of great significance to develop a new type of high-performance corrosion and wear resistant material [5].

In the Al-Ni-Ti ternary system, some binary and ternary intermetallic compounds (NiAl, Ni_3Al, NiTi, Ni_2Ti, Al_2TiNi, Al_3NiTi_2, $AlNi_2Ti$ etc.) have many attractive properties such as high hardness, low density and excellent corrosion and wear resistance [6–8]. As a ternary intermetallic compound with $L1_2$ crystal structure, $AlNi_2Ti$ alloy has higher melting point and strength in Al–Ni–Ti ternary system [9]. Therefore, $AlNi_2Ti$ alloy is expected to have not only good wear resistance due to its inherent high hardness and strong covalent bond atom bonding, but also excellent corrosion resistance due to its high chemical stability and easy passivation of Al, Ni, Ti element composition. However, like other intermetallic compounds, $AlNi_2Ti$ alloy is too brittle for industrial applications. It was found that the strengthening phase $AlNi_2Ti$ and the ductile NiTi can form a coherent interface $AlNi_2Ti$/NiTi multiphase structure, and its room temperature compression strength is as high as 2300 MPa [10]. Moreover, NiTi alloy was also reported to have fairly good wear and corrosion resistance [11]. Sichani et al. [12] have reported that Ni–Al–Ti ternary coatings exhibit better corrosion resistance than Ni–Ti binary alloy coatings due to formation of Al passive film on the surface. Therefore, $AlNi_2Ti$ Heusler alloy with the ductile NiTi as a toughening phase was expected to have an excellent combination of wear and corrosion properties. However, to the author's knowledge, the current researches on NiTi/$AlNi_2Ti$ alloys are mainly focused on mechanical properties, and the researches on its corrosion, especially the tribocorrosion properties (tribocorrosion being simultaneous action of corrosion and wear) are very scarce.

In this paper, a novel NiTi phase toughened NiTi/$AlNi_2Ti$ alloy was designed and prepared by vacuum arc melting. Corrosion and tribocorrosion resistance of the NiTi/$AlNi_2Ti$ alloy was investigated under room-temperature by anodic polarization test and tribocorrosion test, respectively. The chemical composition of the passive film was studied by X-ray photoelectron spectroscopy (XPS). The corresponding corrosion and tribocorrosion mechanisms were discussed.

EXPERIMENTAL

The alloy composition point was designed in the NiTi-$AlNi_2Ti$ pseudo-binary system in the ternary isothermal section of the Al–Ni–Ti system [13]. The nominal composition of the NiTi/$AlNi_2Ti$ is 13.3Al-51Ni-35.7Ti (at %). Alloy ingots are prepared from pure elements (99.8 wt % Al, 99.9 wt % Ni and 99.9 wt % Ti) in a water-cooled copper crucible arc melting furnace with an electromagnetic stirring device under an argon atmosphere. Each ingot was re-melted five times and the ingot was flipped before each re-melting to ensure composition homogeneity. The cast ingots were cut into 10 mm × 10 mm × 5 mm specimens using electro-discharge machining (EDM) for microstructure analysis and tribocorrosion tests.

Microstructure of the NiTi/$AlNi_2Ti$ alloy ingots was characterized using the Olympus BX51M optical microscope (OM) and field-emission scanning electron microscopy (FESEM, JSM-6700F, JEOL, Japan). The phase constituents of the samples were identified by means of X-ray diffraction (XRD, D/Dmax-2400, Rigaku, Japan) with Cu $K\alpha$ radiation (λ = 0.15418 nm). The chemical composition of the phase constituents was analyzed by an energy dispersive spectroscopy (EDS) equipped on the SEM. Volume fraction of the phases in the NiTi/$AlNi_2Ti$ alloy were measured by a image analysis software on high-contrast optical photographs. The hardness of the alloy was measured using a Vickers hardness tester (HVS-1000, Yantai Huayin testing instrument Co., Ltd., China) with a load of 9.8 N and a loading time of 10 s.

The tribocorrosion behaviors of the NiTi/$AlNi_2Ti$ alloy were carried out using a ball-on-flat reciprocating sliding tribometer (MFT-4000, Lanzhou Institute of Chemical Physics, Chinese Academy of Sciences, Lanzhou, China) in 3.5 wt % NaCl solutions. An Al_2O_3 ball (6 mm in diameter) was applied as the wear counterpart due to its high hardness (20 GPa), chemical stability and low electroconductibility, which can effectively reduce the transfer of wear counterpart material to the alloy surface and avoid additional chemical reactions [14]. A normal load 5 N was applied corresponding to the average hertzian contact pressure of 0.97 GPa. The sliding amplitude and frequency were 5 mm and 0.5 Hz, respectively. During the tribocorrosion test, the open-circuit potential (OCP) was recorded for approximately 5 min before a sliding test and then the sliding test continued for 20 min. The OCP recording continued for 5 min after the sliding had ended. At the same time, the current density was continuously recorded under constant potentials during the sliding test. In order to clarify the corrosion-wear synergistic failure mechanism, the sliding in deionized water was carried out under the same test conditions. The coefficient of friction (COF) was recorded in situ. Commercial traditional austenitic stainless steel 1Cr18Ni9Ti with a nominal chemical composition (wt %) of Fe–18.3%Cr–9%Ni–0.5Ti%–0.1%C was selected as a reference material for electrochemical corrosion and tribocorrosion tests. The tribocorrosion products were analyzed by EDS and X-ray photoelectron spectroscopy (XPS).

RESULTS AND DISCUSSION

Microstructure

The typical microstructure of the alloy sample is shown in Fig. 1. It can be seen that the alloy has a uniform and compact microstructure consisting of the primary dendrites and the remaining interdendritic dual-phase structure. EDS analysis indicates that the chemical composition (at %) of the primary dendrites and interdendritic phases is 25.72Al–50.93Ni–23.35Ti and 5.69Al–51.07Ni–43.24Ti, respectively. Combined with the results of XRD analysis (Fig. 1c), it can be confirmed that the primary dendrite is $AlNi_2Ti$ ternary intermetallic, the interdendritic phase is NiTi and Ni_3Ti.

In the Al–Ni–Ti ternary phase diagram, $AlNi_2Ti$ intermetallic has a higher melting point (1500°C) and the large negative free energy of formation in the Al–Ni–Ti ternary system, which causes $AlNi_2Ti$ precipitated firstly from liquid in the rapid solidification process. Following the precipitation of $AlNi_2Ti$ phase, Ni and Ti elements are gradually enriched in residual liquids and transformed into NiTi and Ni_3Ti phases. According to the research of Nash and Liang [15], Ni_3Ti can be further transformed to form $AlNi_2Ti$ and NiTi phases through a peritectic reaction ($L + Ni_3Ti = AlNi_2Ti + NiTi$). However, due to the rapid solidification rate, the peritectic reaction cannot be completely, resulting in partial Ni_3Ti remaining in the product. The volume fraction of the primary dendrite of $AlNi_2Ti$ was determined to be about 61%. The average hardness of the NiTi/$AlNi_2Ti$ alloy was tested to be approximately 736 HV due to the high volume fraction and uniform distribution of the high hardness $AlNi_2Ti$ intermetallic.

Tribocorrosion Behaviors

The tribocorrosion behaviors of NiTi/$AlNi_2Ti$ alloy and 1Cr18Ni9Ti material were investigated under a constant potential condition (or open circuit potential) in 3.5 wt % NaCl solution. Figure 2a shows a typical variation curve of friction coefficient and OCP value for NiTi/$AlNi_2Ti$ alloy in NaCl solution during tribocorrosion test. It can be seen that the change in the OCP value is inversely proportional to the frictional force during tribocorrosion test. The OCP value of the alloy is relatively stable before the start of sliding (soaking), but it decreases significantly with the sliding starts, which can be attributed to the

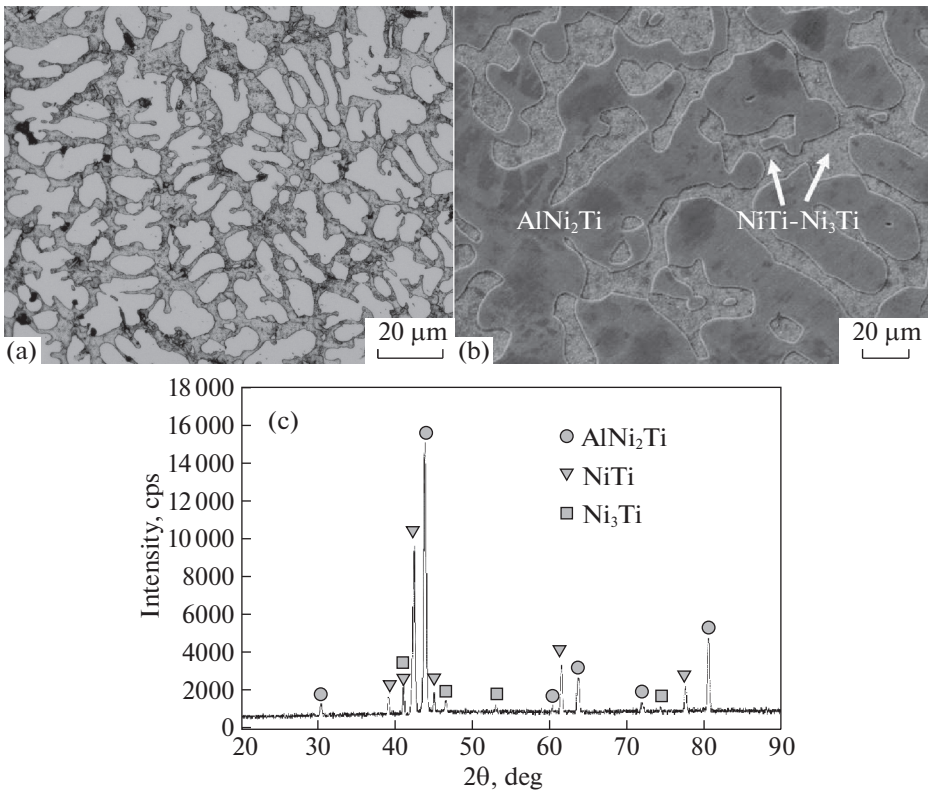

Fig. 1. Microstructure and phase composition of NiTi/$AlNi_2Ti$ intermetallic alloy (a) OM photograph, (b) SEM morphology and (c) XRD pattern.

destruction of the passivation film [16]. When the sliding process has done, the corrosion potential increases significantly due to the strong repassivation ability of the alloy in NaCl solution. For comparison, the tribocorrosion behaviors of 1Cr18Ni9Ti material are similar to that of NiTi/$AlNi_2Ti$ alloy in 3.5 wt % NaCl solution as shown in Fig. 2b. The OCP value decreased markedly during tribocorrosion and increased gradually during passivation due to the synergistic effect of corrosion-wear. However, compared to NiTi/$AlNi_2Ti$ alloy, 1Cr18Ni9Ti material exhibits a higher friction coefficient with a significant fluctuation. The decrease of OCP value from –0.26 to –0.40 V is much larger than that of NiTi/$AlNi_2Ti$ alloy from –0.18 to –0.20 V with the sliding starts, which indicates that NiTi/$AlNi_2Ti$ alloy has better tribocorrosion resistance than 1Cr18Ni9Ti material in 3.5 wt % NaCl solution.

In order to further understand the relationship between corrosion behavior and friction properties, tribocorrosion tests were performed at different polarization potentials as shown in Fig. 3. It can be seen that a significant increase in current is observed during sliding for both specimens. Therefore, corrosion is accelerated by sliding actions, which is observed by many researchers in passive material systems [17]. Under the sliding action, the oxide film at the actual contact position is removed or destroyed after a certain number of sliding cycles, which leads to an increase in the surface area exposed to the solution and accelerated electrochemical corrosion. When the sliding stops, the corrosion current density decreases due to the repassivation of the worn surface. Moreover, as the applied potential increased, the corrosion current of the two materials increases, which indicates that accelerated corrosion of the materials at higher potentials during tribocorrosion test. Compared with NiTi/$AlNi_2Ti$ alloy, sliding leads to a greater increase in current density of 1Cr18Ni9Ti material. The current density of 1Cr18Ni9Ti material is about 2 and 5 mA/cm^2 at applied potentials of 0.2 V (SCE) and 0.5 V (SCE), which is an order of magnitude higher than that of NiTi/$AlNi_2Ti$ alloy at the same corrosion potential.

Figure 4a shows the wear loss volumes of the NiTi/$AlNi_2Ti$ alloy and 1Cr18Ni9Ti material under different potential conditions. The wear loss volumes of the two materials during tribocorrosion in NaCl solution are much higher than that of sliding in deionized water. Moreover, with the increase of applied potential, the wear loss volumes of the two materials increased. In particular, when the application potential is 0.5 V, the wear loss volumes of the two materials are about one order magnitude higher than that of

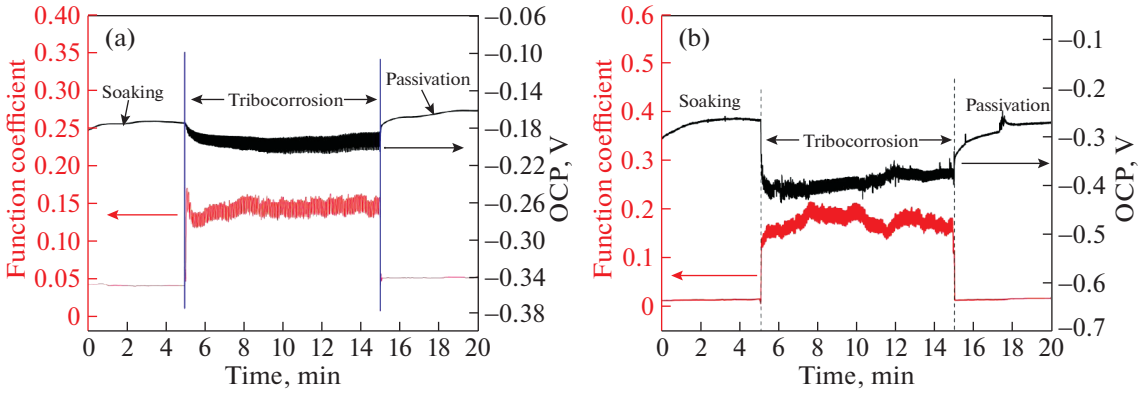

Fig. 2. Tribocorrosion curves with corresponding OCP of NiTi/AlNi$_2$Ti alloy (a) and 1Cr18Ni9Ti reference material (b) in 3.5 wt % NaCl solution.

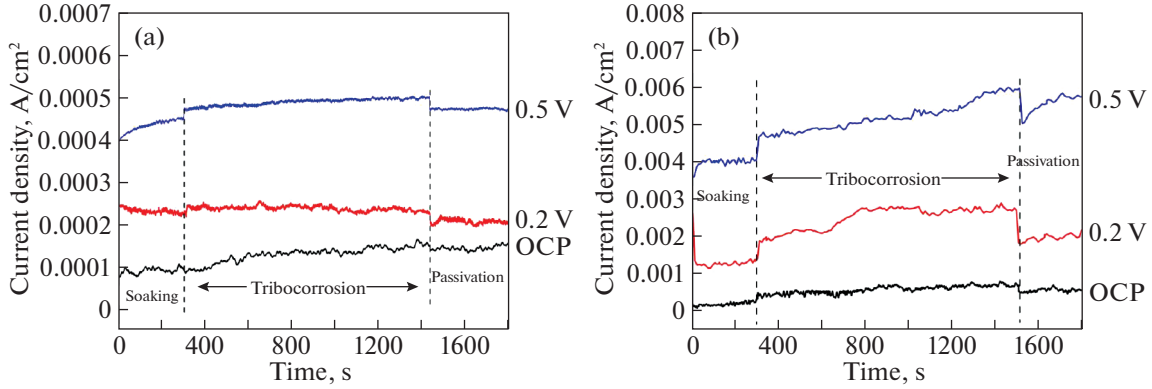

Fig. 3. Current density evolution of NiTi/AlNi$_2$Ti alloy (a) and 1Cr18Ni9Ti reference material (b) under different potential during tribocorrosion test in NaCl solution.

sliding in deionized water, showing a strong wear-corrosion synergistic effect. In addition, the wear loss volume of 1Cr18Ni9Ti material increases much more rapidly than that of NiTi/AlNi$_2$Ti alloy with the increasing applied potential. The wear loss volumes of NiTi/AlNi$_2$Ti alloy are much lower than 1Cr18Ni9Ti material under all applied potential due to higher hardness and higher corrosion resistance.

Chemical composition, compactness is a key factor affecting the stability of the passivation film [18]. After cathode reduction, the change of current with time on NiTi/AlNi$_2$Ti alloy and 1Cr18Ni9Ti material was measured. If the contribution of the double layer charge is neglected, the decrease of current density should be related to the growth of passive film on the electrode surface [2, 19]. The growth kinetics of the passivated film satisfies the Macdonald' s model [20], as follows:

$$I = 10^{-(A+k\log t)}, \qquad (2)$$

where A is a content and k represent the slope of the double-log plot for potentiostatic polarization. Figure 4b shows the double-log diagram of NiTi/AlNi$_2$Ti alloy and 1Cr18Ni9Ti material at 0.5 V vs. SCE potentiostatic polarization measurements in 3.5 wt % NaCl solution. The slopes of the plots (k) for the two materials show a significant variation. For the 1Cr18Ni9Ti material, $k = -0.71$ at the initial formation of the passivation film and $k = -0.42$ at the later stage of the test. For the NiTi/AlNi$_2$Ti alloy, the k values at the initial and late stages of the formation of the passivation film are -0.87 and -1.23, respectively. According to the literature [21], $k = -1$ indicates the formation of a compact and highly protective passive film, while $k = -0.5$ indicates the existence of porous film growth due to the dissolution and precipitation process. Therefore, the passive film formed on the surface of NiTi/AlNi$_2$Ti alloy was more compact than that of 1Cr18Ni9Ti material. Moreover, with the progress of the potentiostatic polarization test, the passive film on the surface of NiTi/AlNi$_2$Ti alloy is gradually compacted, while the passive film on the surface of 1Cr18Ni9Ti material tends to be porous. It can be seen from the above analysis that a compact and stable passivation film was formed on the surface of

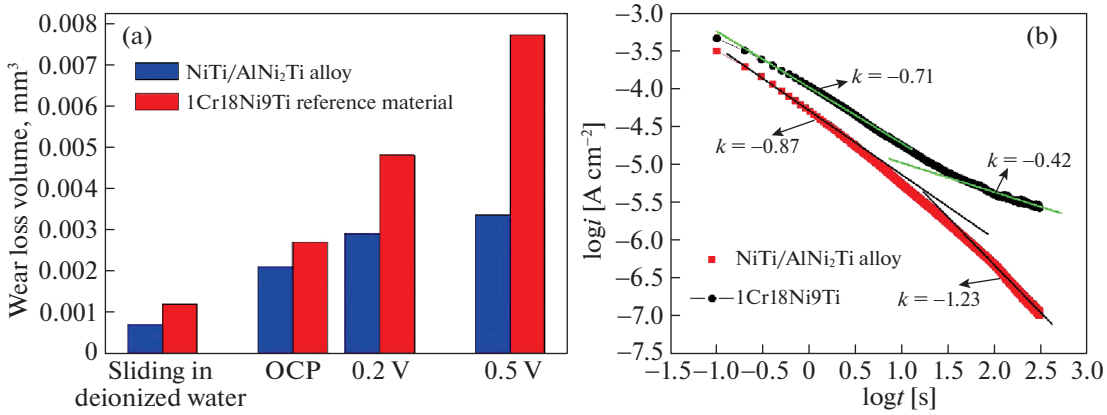

Fig. 4. Total wear loss volumes (a) and double-log plots of current-time (b) for $NiTi/AlNi_2Ti$ alloy and 1Cr18Ni9Ti reference material.

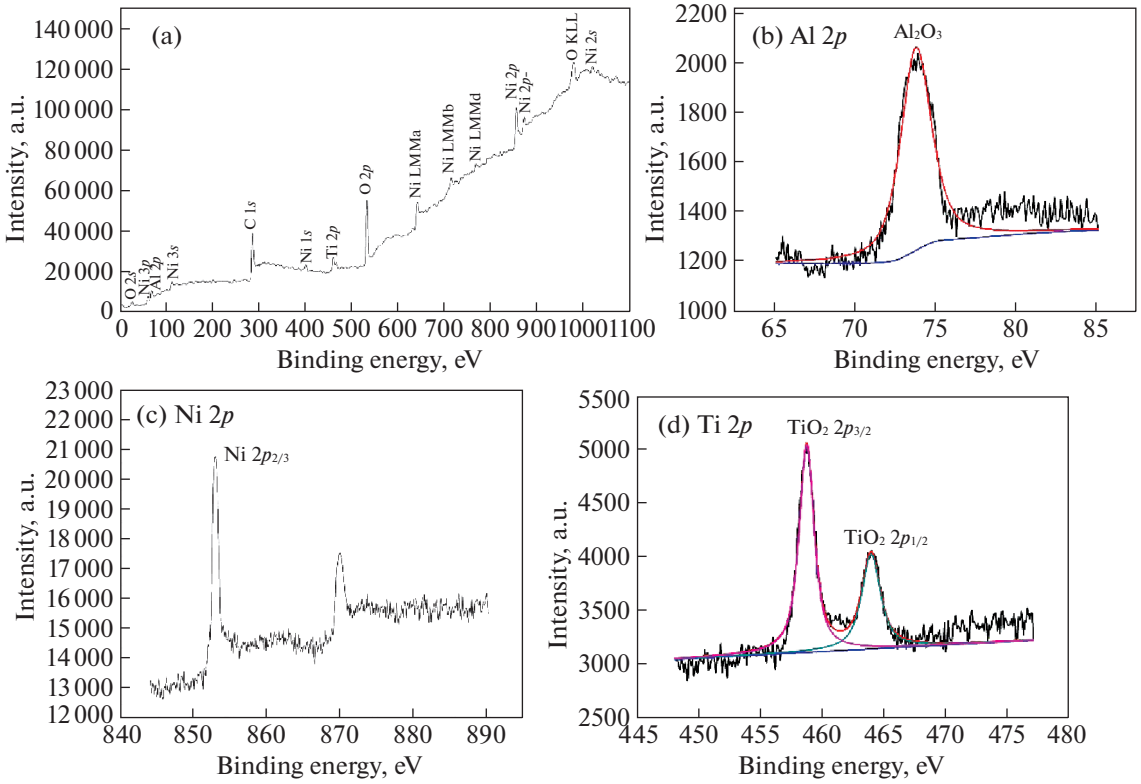

Fig. 5. XPS survey spectra (a) and high-resolution XPS spectra (b)–(d) of the $NiTi/AlNi_2Ti$ alloy after tribocorrosion test in 3.5 wt % NaCl solution.

$NiTi/AlNi_2Ti$ alloy after polarization corrosion, which was also one important reason for the excellent corrosion resistance of the alloy in 3.5 wt % NaCl solution.

In order to better understand the corrosion behavior of $NiTi/AlNi_2Ti$ alloy, it is necessary to determine the chemical composition and chemical state of the elements in the passive film. Figure 5a shows the XPS spectra of $NiTi/AlNi_2Ti$ alloy after tribocorrosion test at applied potentials of 0.5 V in 3.5 wt % NaCl solution. The peaks of Al, Ni, Ti, O and C were detected in the passive film. The C 1*s* peak possibly arises from a contaminant hydrocarbon layer covering the topmost surface of the specimen [22]. In order to further determine the composition of the passive film, the high resolution XPS spectra of Al 2*p*, Ni 2*p* and Ti 2*p* were recorded.

As shown in Fig. 5b, the Al 2*p* spectra shows a single Al 2*p* peak located at a binding energy of 74.5 eV,

indicating that Al is in the form of Al_2O_3 [23]. In Fig. 5c, the Ni 2*p* peak is noticed at a value of 852.5 eV, indicating that the Ni chemical state corresponded to elemental nickel without oxidized contribution [24]. The Ti 2*p* spectrum of the alloy consists of two peaks: Ti $2p_{3/2}$ and Ti $2p_{1/2}$ correspond to Ti^{4+}, and the binding energies are located at 458.68 and 463.98 eV, respectively, indicating that TiO_2 is formed in the passive film [25]. The oxide film in the NiTi/$AlNi_2Ti$ alloy might be recovered by the preferential growth of Al_2O_3 and TiO_2 due to their preferential thermodynamic stability over NiO, as already reported in the literature (free energy of formation $\Delta G^0 = -1676$, -956, and -241 kJ/mol for Al_2O_3, TiO_2 and NiO respectively) [26]. XPS results indicated that the multiphase passive film of Al_2O_3 and TiO_2 was formed on the surface of the alloy after potentiostatic polarization, which makes the alloy have excellent corrosion resistance.

CONCLUSIONS

(1) A novel corrosion-resistant NiTi/$AlNi_2Ti$ intermetallic alloy was fabricated by arc melting process with a microstructure consisting of the primary dendrites $AlNi_2Ti$ and interdendritic phase of NiTi-Ni_3Ti.

(2) With the onset of sliding, the OCP value of NiTi/$AlNi_2Ti$ alloy and 1Cr18Ni9Ti material decreases and the corrosion current density increases during tribocorrosion due to destruction of the passivation film, while the OCP value increases and corrosion current density decreases during repassivation due to the synergistic effect of corrosion and wear. The corrosion current density and wear loss volume of the NiTi/$AlNi_2Ti$ alloy increase with the increase of applied potentials. At potential of 0.5 V, the current density of 1Cr18Ni9Ti material is about one order of magnitude higher than that of NiTi/$AlNi_2Ti$ alloy, and the wear loss volumes of the two materials are about one order magnitude higher than that of sliding in deionized water. NiTi/$AlNi_2Ti$ alloy is more suitable as a tribocorrosion resistance material than 1Cr18Ni9Ti stainless steel.

ACKNOWLEDGMENTS

This research was supported by the Funded by the "Qizhi" Talent Cultivation Project of Lanzhou Institute of Technology (Grant no. 2020QZ-02), Higher Education Innovation Fund Project of Gansu Province of China (Grant no. 2021B-314). The authors acknowledge Lei Huang for their assistance on experiments of arc melting.

SPELL: 1. passivation

CONFLICT OF INTEREST

The authors declare that they have no conflicts of interest.

REFERENCES

1. J. Liu, J. Zhang, L. J. Deng, et al., Surf. Eng. **35**, 59 (2019).
2. L. Yuan and H. M. Wang, Electrochim. Acta **54**, 421 (2008).
3. X. D. Du, J. Q. Wang, G. D. Sun, et al., Mater. Sci. Eng. A **477**, 277 (2008).
4. E. Huttunen-Saarivirta, L. Kilpi, T. J. Hakala, et al., Tribol. Int. **95**, 358 (2016).
5. D. D. Liang, X. S. Wei, T. C. Ma, et al., J. Non-Cryst. Solids **510**, 62 (2019).
6. B. Sefer and S. Virtanen, Corros. Sci. **154**, 287 (2019).
7. G. Song, Z. Q. Sun, J. D. Poplawsky, et al., Acta Mater. **127**, 1 (2017).
8. L. J. Zheng, F. X. Zhang, R. G. Ding, et al., Mater. Des. **110**, 494 (2016).
9. A. D?cebski, W. Gąsior, A. Sypień, et al., Intermetallics **42**, 92 (2013).
10. Y. Koizumi, Y. Ro, S. Nakazawa, et al., Mater. Sci. Eng. A **223**, 36 (1997).
11. M. Farvizi, T. Ebadzadeh, M. R. Vaezi, et al., Wear **334–335**, 35 (2015).
12. H. R. Sichani, M. Salehi, H. Edris, et al., Surf. Coat. Technol. **309**, 959 (2017).
13. J. C. Schuster, Z. Pan, S. H. Liu, et al., Intermetallics **15**, 1257 (2007).
14. T. Shao, F. F. Ge, Y. Dong, et al., Wear **416–417**, 44 (2018).
15. P. Nash and W. W. Liang, Metall. Trans. A **16**, 319 (1985).
16. F. Pougoum, J. C. Qian, L. Martinu, et al., Surf. Coat. Technol. **357**, 774 (2019).
17. Y. Sun and E. Haruman, Surf. Coat. Technol. **205**, 4280 (2011).
18. Y. Wang, S. L. Jiang, Y. G. Zheng, et al., Corros. Sci. **63**, 159 (2012).
19. L. Liu, Y. Li, and F. H. Wang, J. Mater. Sci. Technol. **26** (1), 1 (2010).
20. H. H. Hassan, Electrochim. Acta **51**, 526 (2005).
21. L. Liu, Y. Li, and F. H. Wang, Electrochim. Acta **53**, 2453 (2008).
22. M. Fazel, H. R. Salimijazi, and M. Shamanian, ACS Appl. Mater. Interfaces **10**, 15281 (2018).
23. J. Xu, L. L. Liu, P. Munroe, et al., J. Mater. Chem. A **1**, 10281 (2013).
24. L. Yuan and H. M. Wang, Intermetallics **16**, 1149 (2008).
25. Q. Chen, Z. W. Xie, T. Chen, et al., Materials **9**, 963 (2016).
26. P. Močnik, T. Kosec, J. Kovač, et al., Mater. Sci. Eng. C **78**, 682 (2017).